Journal of Molecular and Cellular Cardiology 58 (2013) 13–21

Contents lists available at SciVerse ScienceDirect

Journal of Molecular and Cellular Cardiology

journal homepage: www.elsevier.com/locate/yjmcc

Review article

# Superresolution microscopy in heart — Cardiac nanoscopy

Tobias Kohl [a,b], Volker Westphal [c,e], Stefan W. Hell [a,c,e], Stephan E. Lehnart [a,b,d,e,*]

[a] Heart Research Center Goettingen, University Medicine Goettingen, Germany
[b] Department of Cardiology & Pulmonology, University Medicine Goettingen, Germany
[c] Department of NanoBiophotonics, Max Planck Institute for Biophysical Chemistry, Goettingen, Germany
[d] Center for Biomedical Engineering and Technology, University of Maryland Baltimore, USA
[e] DZHK (German Centre for Cardiovascular Research) site Goettingen, Germany

ARTICLE INFO

*Article history:*
Received 30 July 2012
Received in revised form 3 November 2012
Accepted 24 November 2012
Available online 3 December 2012

*Keywords:*
Calcium
Excitation–contraction coupling
Cell biology
Heart failure
Superresolution
Fluorescence microscopy

ABSTRACT

Detailed understanding of the adaptive nature of cardiac cells in health and disease requires investigation of proteins and membranes in their native physiological environment, ideally by noninvasive optical methods. However, conventional light microscopy does not resolve the spatial characteristics of small fluorescently labeled protein or membrane structures in cells. Due to diffraction limiting resolution to half the wavelength of light, adjacent fluorescent molecules spaced at less than ~250 nm are not separately visualized. This fundamental problem has lead to a rapidly growing area of research, superresolution fluorescence microscopy, also called nanoscopy. We discuss pioneering applications of superresolution microscopy relevant to the heart, emphasizing different nanoscopy strategies toward new insight in cardiac cell biology. Here, we focus on molecular and structural readouts from subcellular nanodomains and organelles related to $Ca^{2+}$ signaling during excitation–contraction (EC) coupling, including live cell imaging strategies. Based on existing data and superresolution techniques, we suggest that an important future aim will be subcellular in situ structure–function analysis with nanometric resolving power in organotypic cells. This article is part of a Special Issue entitled "Calcium Signaling in Heart".



**Contents**



## 1. Introduction

Fluorescence light microscopy is central to elucidate and understand cellular functions. Conceptually, it represents a combined strategy to visualize molecules or cells by specific labeling with small fluorescent molecules or fluorescent proteins (FPs), subsequently characterized by optical image acquisition and analysis. This includes imaging of endogenous proteins in the typical membrane environment of living cells, and can be extended by certain strategies to single molecules.

Nowadays laser scanning confocal and multiphoton fluorescence microscopes represent the standard tools of cell biology research. Compared to wide-field imaging, these strategies reduce out-of-focus fluorescence through defined optical sections inside specimens.

* Corresponding author at: University Medicine Goettingen, Dept. of Cardiology & Pulmonology, Robert-Koch-Str. 40, 37075 Goettingen, Germany. Tel.: +49 551 39 10575; fax: +49 551 39 10650.
*E-mail address:* slehnart@med.uni-goettingen.de (S.E. Lehnart).

0022-2828/$ – see front matter © 2012 Elsevier Ltd. All rights reserved.
http://dx.doi.org/10.1016/j.yjmcc.2012.11.016

Nevertheless these conventional approaches are significantly limited in resolving power to several hundreds of nanometers due to light diffraction. This fundamental resolution limit (~250 nm) corresponds roughly to the dimensions of mitochondria (Fig. 1A), which is not sufficient to characterize the intricate architecture of small organelles inside cardiomyocytes. Obviously, microdomains and organelles with sizes smaller than the resolution limit cannot be characterized in detail or discriminated at high spatial densities (Fig. 1B). This important issue has significantly limited a more detailed, molecular understanding of subcellular structures and highly localized in situ functions of intact cells by fluorescence microscopy.

Recent developments have led to fundamentally new microscopy techniques, which effectively overcome the resolution barrier even toward lower nanometer scales [1,2]. It is important to note that light diffraction, the interference of light waves with the optical parts of the far-field microscope, cannot be avoided. Therefore, during image acquisition fluorescent point emitters are registered as spatially spread out signals (Fig. 1B). Accordingly, this behavior is characterized by the point spread function (PSF) that depends on the wavelength of light ($\lambda$) and the optical properties of the microscope objective (numerical aperture, NA). The size of the point spread function is typically described by full width at half maximum (FWHM) and expands several hundred nanometers laterally (~250 nm in x/y, given by $FWHM \approx 0.6 \cdot \lambda / NA$) and axially (~600 nm in z, given by $FWHM \approx n \cdot \lambda / NA^2$; n, refractive index). Since two or more point emitters closer to each other than the PSF width at half maximum typically occur in a fluorescently labeled cell, nearby fluorescent markers appear as one blurred imaging object, but are not resolved individually.

In contrast, superresolution techniques circumvent the diffraction limit, thereby improving resolution by one order of magnitude or more, either by turning on and off molecules individually followed by high precision localization (stochastic spatial coordinate) or by turning them on and off in predefined nano sized areas in space [2,3]. Both approaches use state transitions of fluorophores to keep the majority of molecules within the diffraction-limited volume dark or non-responsive to excitation light (targeted spatial coordinate). Since both schemes have been successfully applied to cardiac samples recently [4–6], this topical review outlines the application of nanoscopy techniques for cardiac cell biology.

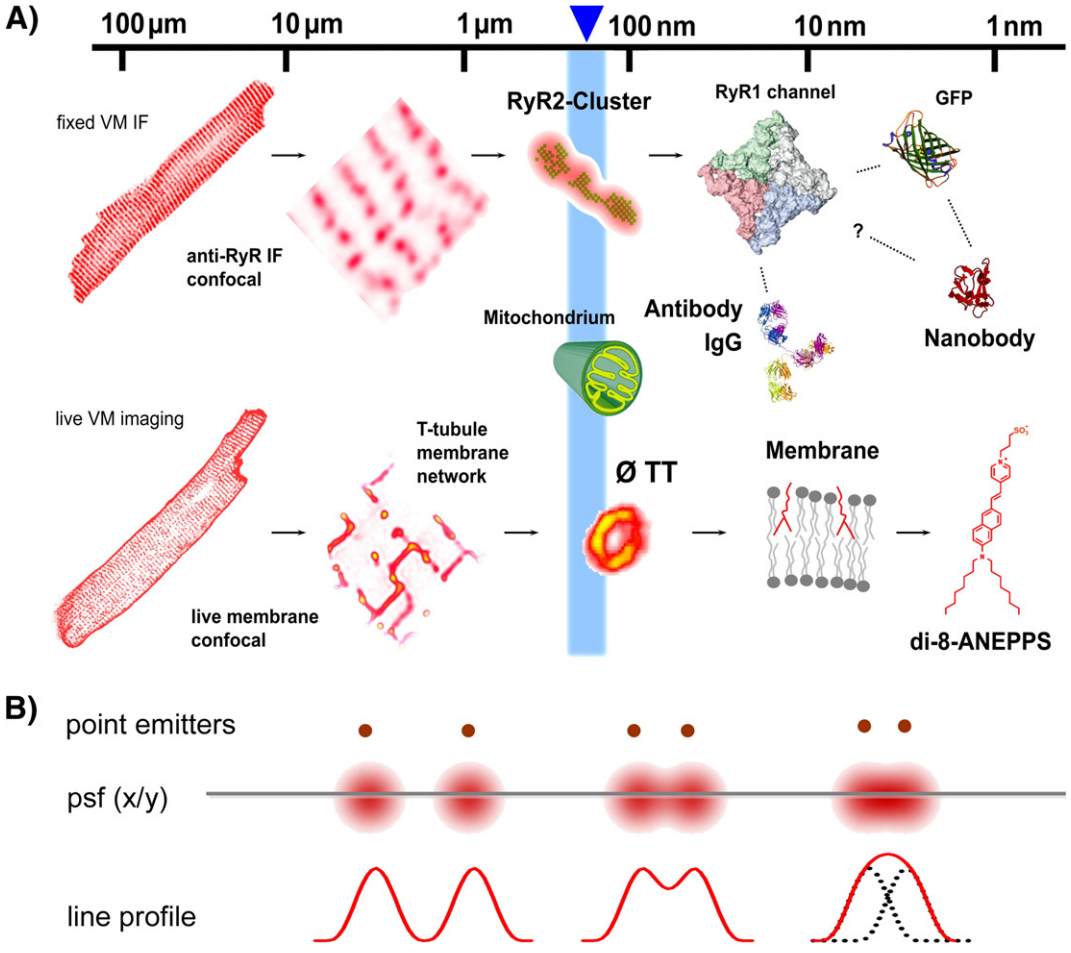


**Fig. 1.** Essential membrane structures and $Ca^{2+}$ transport proteins of cardiomyocytes in relation to optical resolution scales. A) The cellular organization of membrane structures, $Ca^{2+}$ binding proteins, and targeting of fluorescent probes occur at different scales in a ventricular myocyte (VM). The diffraction limit of resolution (indicated by vertical blue bar) highlights examples of cellular structures that benefit from superresolution microscopy through detailed image information. From left to right: VM, confocal image of a VM cell showing the typical transversal striation pattern; TT membrane network labeled with di-8-ANEPPS [4]; RyR2 cluster, individual channel shapes (green) fitted into a reconstructed superresolution image (not shown) compared to the diffraction limited signal (red) [6]; mito, cartoon of cross-sectioned mitochondrial organelle showing cristae structures of the inner membrane (yellow) [99]; ∅TT, individual hollow TT membrane cross-section resolved by STED [4]; RyR1, cryoEM domain model for RyR1 channel tetramer showing a 27×27 nm sized cytosolic surface structure [100]; IgG, immunoglobulin G ribbon representation (PDB: 1IGT); GFP, molecular β-barrel structure [101]; nanobody, an anti-GFP based superresolution marker strategy [55]; Membran, cartoon of the lipid bilayer with intercalated di-8-ANEPPS molecules ordered according to approximate scale size. B) Optical resolution is limited by light diffraction. The optical resolution depends on the size of the effective point spread function (PSF) as shown in the imaging plane (x/y). Due to light diffraction, two sufficiently close point emitters are detected as ensemble (blurred) signal of two combined PSF signal distributions (right case). Only point emitters spaced at a sufficient distance can be discriminated due to light diffraction (left case). Note: the optical resolution principles discussed here differ from the single-molecule localization principles discussed in Section 3.

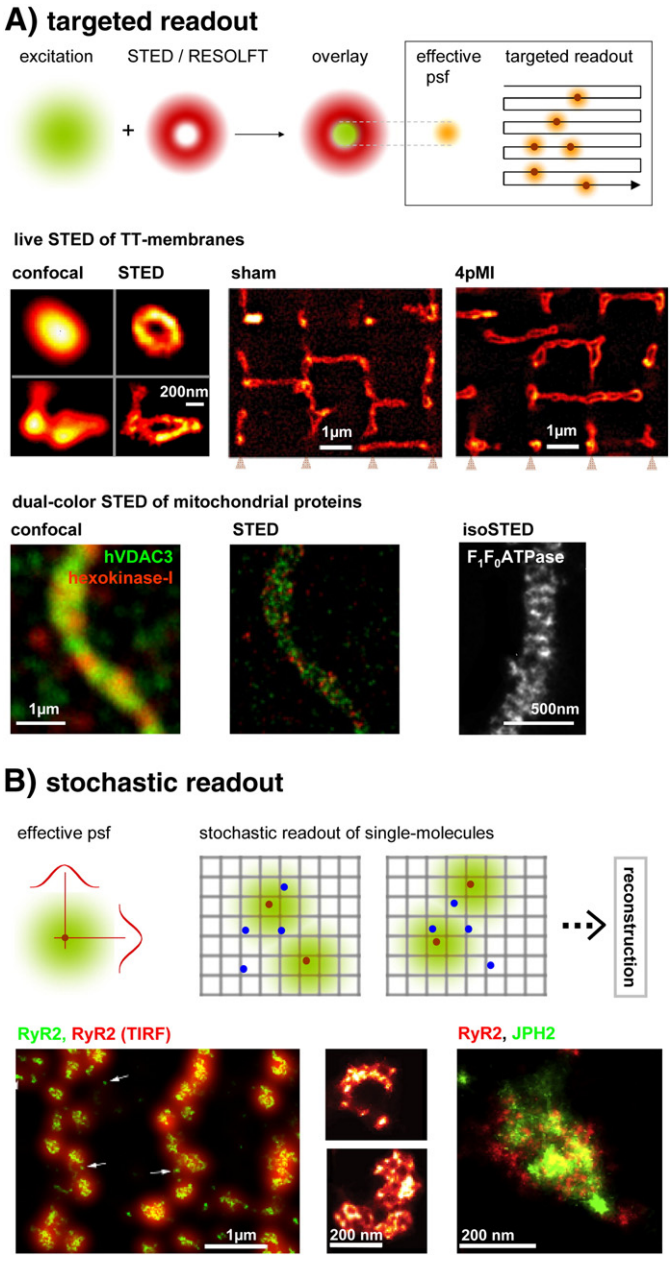


**Fig. 2.** Strategies and applications for superresolution microscopy in cell imaging. A) Targeted readout. Top: Photo-switching with STED or RESOLFT is targeted to the spot of focused excitation light (green). A toroid shaped laser beam (red) spatially confines the central signal, thereby reducing the effective PSF size below the diffraction limit. Right box: In targeted readout, laser scanning of the sample by the overlaid excitation and photo-switching laser beams directly produces the superresolution image from the given cellular imaging plane. Center: Using STED, important details of individual TT membrane cross-sections as well as the cell-wide membrane network were resolved in living cardiomyocytes, which facilitated identification of early changes of intact membranes 4 weeks post-MI (4pMI) compared to sham hearts [4]. Lower: dual-color STED resolved the separation of the indicated mitochondrial proteins in cultured cells [32] and 3D superresolution isoSTED identified cristae structures at the inner mitochondrial membrane [99]. B) Stochastic readout. Top: Photo-switching results in stochastic behaviors defined by groups of inactive (blue) and active (red) single-molecule fluorophores. For random single molecule emissions to be detected as individual diffraction-limited signals (effective PSF), a relatively high number (up to 100,000) of sequential wide-field imaging frames are captured. Individual molecule localizations are determined by signal fitting for each subdiffraction frame and reconstruction of the final superresolution image. Lower: The examples show the distribution and morphology of peripheral RyR2 clusters at the cardiomyocyte surface (left); complex RyR2 super-cluster shapes and heterogeneous signal patterns (center); and the colocalized distribution of RyR2 and JPH2 proteins within clusters [5,6].

While distinct conceptual terms describe the individual superresolution methods, here we compare the main working principles of 'targeted' versus 'stochastic' readouts [1,3]. A targeted readout is based on optically engineered (structured) illumination patterns, which precisely define where fluorophores can assume the fluorescent state (Fig. 2A, *top*). Targeted approaches include the first super-resolution concept, stimulated emission depletion (STED) [7,8], the related reversible optically-linear fluorescence transitions (RESOLFT) [9], and structured illumination microscopy (SIM, SSIM) [10–12]. In contrast, for stochastic readout fluorescent molecules are switched randomly to the fluorescent state and localized individually with nanometer precision; after registration the molecules are turned off. The superresolution image is then reconstructed from a sufficiently large set of captured frames containing the fluorophore localization data. Stochastic optical reconstruction microscopy (STORM), photo-activation localization microscopy (PALM), fluorescence-PALM (F-PALM), and ground-state-depletion with individual molecule return (GSDIM) [13,14] are examples for applications which randomly switch fluorophores.

Recently, a targeted readout using STED superresolution microscopy has resolved intact T-tubule membrane structures deep inside living cardiomyocytes for the first time [4]. Furthermore, a stochastic readout has been successfully established for ryanodine receptors (RyR2s) at the surface of cardiomyocytes, referred to as 'peripheral' clusters [5,6,15]. From a general perspective, such superresolution techniques will have a major impact on future understanding and interpretation of cardiac cell biology, particularly at the level of subcellular structures and spatially confined signal processes. We summarize recent super-resolution developments, discuss relevant limitations, and highlight existing cardiac or related applications. In particular, we focus on organelles and nanodomains associated with EC coupling mechanisms, which are not resolved by conventional microscopy techniques.

## 2. Targeted readout: STED, RESOLFT, and SSIM

Targeted fluorescence readout by STED and RESOLFT achieves nanometric image resolution by a common principle (Fig. 2A *top*): while fluorescent molecules are transferred to a fluorescent state (switched on) within the focal spot, a second laser is overlaid providing a spatially defined intensity distribution featuring an intensity zero. The second laser typically switches off all peripheral (non-center) fluorophores but not those located at the intensity minimum (e.g. by STED). For this, the second laser beam is usually shaped like an axially elongated toroid [3,7–9,16] with a central minimum of intensity (<1%) at the focal center (resembling a doughnut in the focal plane). If the STED laser intensity is sufficiently high, fluorescent molecules are confined to the (central) intensity zero, while any peripheral molecules are effectively switched off. As the toroid beam is limited by diffraction, increasing the STED laser intensity spreads the region where peripheral fluorophores are switched off, both inwards and outwards. Ultimately, the effective spot size, i.e. the region in which molecules can assume the fluorescent state, is reduced below the diffraction limit, which significantly increases lateral resolution down to nanometric sizes (for diffraction unlimited resolution). Unless additional strategies to simultaneously improve the axial resolution are applied (see below), a pinhole reduces out of focus fluorescence resulting in a *z*-resolution similar to confocal laser scanning microscopes. For STED, laser scanning through overlaid beams across a cellular region of interest generates a superresolution image as direct readout. Additionally, imaging speed has been increased through parallelized multiple foci [17] or through striped illumination patterns in RESOLFT [18].

In small, isolated cells STED imaging has achieved a lateral resolution of ~20 nm, in relatively large cardiac myocytes ~55 nm, and a resolution of ~70 nm was achieved in the intact brain of the living mouse [4,19,20]. Furthermore, time-gated acquisition in STED microscopy improved the image contrast, resulting in a comparable

resolution but at a significantly lower STED laser intensity [21]. Considering strategies to further increase resolution, the signal to noise (S/N) ratio will be a limiting factor, since increasingly smaller amounts of fluorophores are detected from a smaller effective PSF. Furthermore, the photostability of the fluorophore and potential light scattering, particularly if imaging occurs deep within the sample, will limit effective resolution by the maximally applicable STED laser power. Therefore, the resolution achieved by STED imaging will directly benefit from bright and photostable dye molecules and a relatively high number of fluorophores detected simultaneously. Accordingly, staining strategies which use markers at high concentrations result in a high S/N ratio, while detection and discrimination of individual molecules, e.g. membrane localized proteins, will benefit from a high labeling ratio (a high number of fluorophore markers per target molecule). An apparent advantage, many different organic dyes and fluorescent proteins undergo nonlinear fluorophore transitions during application of the STED beam [19,22–28]. In contrast, RESOLFT is based on reversibly photo-switching FPs at several orders of lower light intensity based on long-lived dark states [3,9]. Therefore, RESOLFT will effectively avoid photo-damage and multiphoton induced dye bleaching, a clear advantage if imaging of particularly sensitive properties or time-lapse imaging of living cells is critical.

A common confocal application, multi-color imaging has also been realized in superresolution microscopy. Accordingly, different dual color STED approaches exist that differ by number and combination of laser lines for excitation and depletion [25,29–32]. For example, dual color STED approaches used either the same or different laser wavelengths to switch the dye fluorescence off. Using different STED laser configurations, it was shown that the voltage-dependent anion channel (VDAC) does not co-localize with the enzyme hexokinase in the mitochondrial outer membrane [32].

While membrane domains can be sufficiently approximated by planar geometries [6], cellular structures occur necessarily also in three dimensions. Accordingly, imaging schemes were developed to extend STED superresolution along the optical axis ($z$). For example, using two oppositely aligned lenses, isoSTED resolved the cristae of the inner mitochondrial membrane in 3D at ~30 nm resolution in all directions [30]. Alternatively, the intensity distribution can be switched both along the optical axis and laterally using an 'optical bottle beam' [33,34], which can be combined with STED microscopy to simultaneously improve lateral and axial resolution [28,35,36]. Measuring fluorescent beads, a combined lateral and axial resolution of 43 nm and 125 nm has been achieved [36]. Furthermore, bottle beam configurations work as standalone or in combination with the above described lateral toroid to design a resolution scheme targeted at the biological structure of interest, as reported for living cell images at ~150 nm axial resolution [28].

In contrast to STED and RESOLFT, saturated structured illumination microscopy (SSIM) combines widefield imaging with patterned excitation light resulting in ~50 nm lateral resolution [12]. SSIM is an extension of structured illumination microscopy (SIM), which uses a diffraction-limited illumination pattern, varied in space to confine the size of the fluorescent focal spots. Using repetitive imaging and image reconstruction, SIM improved the lateral resolution ~2-fold up to ~100 nm laterally and ~300 nm axially [10,37]. To achieve SSIM-type superresolution, analogous to STED a saturable fluorescent process i.e. a molecular transition from an off to an on state or vice versa is modulated by light intensity in addition to the above mentioned SIM scheme [11]; in essence SSIM is the same concept as the RESOLFT when line structures are used in the latter. In summary, a variety of commercial and custom-designed strategies and validated applications exist, which provide abundant opportunities for targeted superresolution studies.

## 3. Stochastic readout: superresolution by single molecule imaging

Image generation from stochastic readouts also occurs through a multistep procedure. To detect individual fluorescent molecules during wide-field illumination, the majority of fluorophores is maintained in a dark state. Ideally, the result is a sufficiently sparse population of randomly blinking single molecules, where individual signals are captured by a sufficiently large number of frames (1000–100,000), each representing a randomly blinking individual fluorophore. For each frame, the exact localization of individual fluorophores is determined, and reconstruction yields the final superresolution image (Fig. 2B *top*). Superresolution strategies to modulate fluorescent emission for stochastic readout include photo-switching, photo-activation or reversible photo-bleaching which depend on the dye properties. Accordingly, several approaches based on different photomodulation schemes and for different dyes have been established: STORM [38], PALM [39], FPALM [40], PALMIRA [41], GSDIM [13,14] and BALM [42]. see also table of non-standard abbreviations.] Notably, both synchronized and asynchronous photo-activation strategies have been realized [38–41]. While stochastic approaches are generally less equipment intense compared to targeted readout strategies, they require additional analytical expertise and multiple readout steps leading to an overall increased image acquisition time.

Importantly, precise localization of individual fluorophores in densely labeled samples is only possible when photo-modulation switches off (keeps dark) a sufficiently high number of molecules (Fig. 2B *top*). Only then will randomly distributed individual fluorophores occur with sufficiently high spacing to be identified considering diffraction limitations. Accordingly, stochastic approaches have achieved a lateral image resolution of up to ~20 nm [38]. Both the precision of single-molecule localization and the number of localized signals within a given structure (the labeling or localization density) affect the final image resolution and accuracy [43]. Localization precision depends on the fluorophore brightness and exposure time, since fluorophore positions can be determined approximately $\sqrt{n}$ times more precise than the diffraction limit, where $n$ is the number of photons detected by one acquisition frame. For object reconstruction with highest resolution (20 nm), labeling densities of up to $10^4$ fluorophores/$\mu m^2$ may be necessary, which further depend on the geometry of the target structure [1], to avoid spatial under-sampling. Vice versa, for high labeling densities the possibility of imaging artifacts has been considered if the fluorescent markers are not completely off, resulting in insufficient switching-contrast [1]. One concern of denser fluorophore emissions is that high-precision localization is prevented. It has been pointed out, that single-molecule imaging approaches might be particularly advantageous for small or filamentous objects rather than dense and bulky structures [2], although possible limitations should be determined empirically.

Meanwhile single-molecule based approaches are routinely used for 3D imaging. Among the imaging schemes applied are astigmatism, two-focal-plane imaging, and a phase ramp approach [1,44]. These strategies resulted in localization accuracies of ~50 nm in $z$-direction [1,45], within the focal depth of a few hundred nm. As a general rule, 3D imaging with single-molecule strategies is relatively slow and therefore particularly sensitive to any form of sample drift. Initial 3D imaging with PALM showed the molecular architecture of the focal adhesion core region connected to integrin and actin [46]. Imaging objects several microns deep in primary cardiomyocytes or tissue slices may suffer from a decreased S/N ratio and increased light scattering limiting localization accuracy. Nevertheless, stochastic superresolution images from cardiac tissue slices have been achieved, including RyR2, calsequestrin and microtubule protein structures [15,44].

While most stochastic superresolution microscopy has been conducted in chemically fixed cells, some groups have recently extended imaging efforts to live cells. STORM mainly used photo-chromic (rhodamine or diarylethene) and photo-switchable (cyanine) dyes, whereas PALM and FPALM employed photo-activatable fluorescent proteins (e.g. Eos2, Dronpa and PS-CFP2). Dual and even multi-color imaging for stochastic readout is well established and is promising to elucidate cardiac microdomain architectures and compositions. If multiple

fluorophores are used, their relative positions can be determined through spectral separation of the different emission colors [47,48] or through sequential photo-activation or deactivation [49–51]. Furthermore, new multi-color applications are continuously developed and improved [52,53]. Important examples of single and dual-color approaches from cardiac samples will be discussed under Section 5 and after further consideration of fluorescent probe strategies.

## 4. Fluorescent probes and subcellular protein targeting for superresolution imaging

As outlined above, superresolution imaging is intricately linked not only to photo-physical dye properties, but also to the subcellular environment of the proteins and membranes which are marked by fluorophores. Live cell imaging and multi-color applications depend critically on the availability of suitable combinations of dye and laser properties as well as efficient labeling strategies. Comprehensive reviews of suitable dye systems for superresolution have been presented [1,54]. Of note, commonly used IF protocols in fixed samples benefit from a large choice of established organic fluorophores linked to secondary antibodies. Many organic dyes show sufficiently high photon emission and photostability for superresolution. However, IF labeling with antibodies (150–160 kDa) can be inefficient due to high background signals, invasive protocols and inherent 'linkage errors'. Linkage errors of 20 nm and more result from the displacement of fluorophores from the actual epitope inherent to 1ary/2nry antibody complexes with individual steric sizes of 10–15 nm (Fig. 1A) [55]. Alternatively, labeled Fab-fragments (~50 kDa) can help to minimize linkage errors, if trade-offs such as higher costs and additional technical challenges are acceptable.

In contrast, genetic targeting of FPs occurs directly and in live cells. Ongoing progress includes the development and optimization of photo-activatable and photo-switchable proteins [54]. Genetic targeting is by nature specific and provides a defined molecular labeling ratio of FPs relative to the protein of interest. Yet, relatively low molecular labeling ratios compared to standard IF approaches may limit the sample brightness and labeling density. Alternatively, genetic labeling has been combined with organic dyes. Target proteins have been genetically fused to small affinity tags or enzymes that bind modified fluorophores at the surface or after intracellular delivery of the probes, e.g. SNAP or CLIP [54]. Recently, anti-GFP single-domain antibody fragments, nanobodies (12–15 kDa) less than 3 nm in dimension, have been shown to label GFP-fused proteins with linkage errors below 5 nm [55]. This approach also confirms the potential of directly labeled small Fab-fragments. For studies of primary cells like cardiomyocytes, however, genetic targeting requires either transgenic mouse strategies or extended cell culture for viral gene transfer. Another strategy used exogenous application of the recombinant, fluorescently labeled FKBP protein in permeabilized cells as an affinity probe for the RyR2 channel complex [56].

Using small organic dyes, specific membranes or organelles can be labeled in cells. Among a variety of established dyes which are commercially available, several photo-switchable compounds have been established. The membrane probe di-8-ANEPPS, which partitions into the outer membrane leaflet, was successfully used for STED superresolution microscopy of intact membranes (see below) [4]. Additionally, membrane and organelle markers were used with STORM for dynamic imaging in live cells with 30–60 nm spatial and 1–10 sec temporal resolution of [57]. In summary, available organic and genetically encoded fluorophores allow for superresolution imaging of cells including dual-color applications.

Given sufficient labeling density, the fluorophore location and spacing represent the structure of interest and ideally match in scale with the superresolution approach. For STED, the optimal labeling density has been established empirically to image centrioles with a known molecular structure [58]. While under-labeling resulted in incomplete detection of centrioles, over-labeling resulted in blurred substructures, falsely suggesting non-existing image information. Similar over- and under-labeling artifacts may occur during stochastic readout superresolution (as discussed in Section 3). Interestingly, defined subcellular imaging volumes (e.g. organelles, dendrites) marked with FPs at high densities will favor an improved S/N ratio and image accuracy, yet at the same time may be limited during repetitive stochastic sampling due to inadvertent movement or unresolved fluorophore aggregates. Moreover it is not clear whether all epitopes within a cell's nanodomain or a multimeric protein complex are equally accessible to antibody based markers. Remarkably, nanoparticles with over 3 nm size applied in immunogold labeling of permeabilized cardiomyocytes showed limited access to the dyadic subspace, the nanodomain gap between the T-tubule membrane and the junctional SR [59]. Consequently, inadvertent heterogeneity of labeling due to size limited access to subcellular compartments is defined by specific cell architectures and is a concern for superresolution imaging. In practice, the accuracy of the image information will depend on opto-physical parameters of the imaging scheme, the labeling efficiency and density, and the correct subcellular targeting of stable bright fluorophores.

## 5. Microscopy studies with immediate implications for cardiac nanophysiology

EM studies have assessed the architecture of key intracellular membrane compartments like the $Ca^{2+}$ release unit (CRU) and T-tubules (TTs) based on invasive protocols as a necessary prerequisite for sample preparation [60–62]. In parallel, studies on the partitioning and spatial relations of different membrane proteins in the cardiac CRU have been limited to confocal image resolution in the context of IF studies based on membrane permeabilization protocols [63–67]. In contrast, the morphology of the TT membrane structures at the level of individual membrane sheets or tubule cross-sections is not accessible to conventional optical imaging. Nevertheless, indirect TT network analysis based on cell-specific periodic signal patterns (striations) and changes in disease resulted in important insight [68]. Common membrane labeling methods include live cell staining (ANEP dyes), indirect (negative) staining based on the TT contained diffusion space filled with fluorescent dextran conjugates, fluorescent WGA surface conjugates, or anti-Cav3 antibodies to mark the membrane space in fixed cells [63,67,69–71]. We will extend this topic in Section 7.

A direct physiological readout, the subcellular $Ca^{2+}$ release events known as 'elemental' $Ca^{2+}$ sparks have revolutionized our understanding about CRU function both in health and disease. $Ca^{2+}$ spark measurements are based on millisec fast confocal measurements of highly localized release events [72], further combined with negative TT staining for structure–function analysis [73], and recently combined with intraluminal $Ca^{2+}$ release dynamics inside the junctional sarcoplasmic reticulum (jSR) [74]. Furthermore, intracellular voltage imaging in live cells was extended through novel voltage-sensitive dyes and fast random-access microscopy to sample from multiple TT membrane positions for voltage signals [69,75]. Although we can consider only on a limited number of studies here, it is apparent that detailed investigation of nanodomains at the scale of cardiac CRU structures is an important area for superresolution studies.

## 6. Superresolution imaging in living cells

Live cell superresolution imaging allows one to directly gain structural and/or dynamic information from the intact subcellular environment. This includes monitoring of the structural plasticity or dynamic signaling events confined to the nanoscale. Due to the live cell paradigm the potential for artifacts from sample fixation, permeabilization, dehydration, sectioning, and/or cell-fractionation protocols is avoided altogether. Compared to standard microscopy, live cell imaging for

super-resolution faces three general challenges: 1) common to all superresolution schemes, a majority of fluorophores within the diffraction limited volume are kept in a dark state, therefore increasing acquisition time; 2) nanometric resolution demands finer sampling, either by finer steps during scanning or by a higher number of fluorophore localizations to fulfill spatial sampling requirements; 3) on the other hand, nanometric resolution demands faster image acquisition to minimize an increased risk of motion artifacts at nanometric scales. An important concern, when visualizing smallest objects at nanometric scales, the higher sensitivity will also amplify any inadvertent object movement.

In order to minimize artifacts from inadvertent sample movements or during repeated sampling of dynamic events over time, temporal resolution has to be optimized using a trade-off with spatial resolution. For stochastic readout this trade-off is defined by the molecular photon count related to the frame exposure time and fluorophore brightness, by labeling density, and by dye switching rates (see also Section 3). For targeted readout with STED and RESOLFT the field of view can be negotiated against the frame rate of image acquisition to achieve a higher temporal resolution. Notably, for point-scanning techniques, the relevant time-scale for blurring due to motion artifacts is the line, but not the frame acquisition time, the former being significantly shorter. In practice, possible photo-damage in sensitive living samples by high-intensity photo-switching laser light, effects of light scattering deep inside cells, the brightness of fluorophores, and the labeling density all require empirical in situ testing, and if feasible the application of calibration tools.

Notably, STED imaging was recently significantly extended by measurements deep inside living cells and tissues [4,20], where the spatial and temporal resolution increasingly depends on the brightness and size of the imaged objects. Importantly, video rate STED imaging with 28 frames/s at 62 nm spatial resolution has been demonstrated during trafficking of synaptic vesicles with bright labeling through endocytosed antibodies [76]. Slower time-lapse imaging with STED and RESOLFT was accomplished with FP based volume stains of the ER or dendritic spine at resolutions below 70 nm [24,77,78], frame acquisition times of ≤ms [24], or 10–15 μm below the brain surface [77]. Furthermore, live STED dual-color applications with ~80 nm lateral resolution have been reported based on advanced labeling strategies with photo-chromic FPs, combinations of YFP and GFP, and hybrid labeling using SNAP and CLIP [79,80].

For stochastic superresolution readout, image acquisition times from seconds to minutes have been reported. The read-out time for single-molecule approaches depends critically on the switching and emission rates of the dye molecule. As a consequence macromolecular structures with a relatively slow molecular turnover have been successful substrates for single-molecule based approaches, for example focal adhesion molecules or microtubules. To address potential artifacts due to sample drift during longer acquisition times, imaging routines which correct for sample drift have been implemented [38]. Recently, live imaging for stochastic readout has taken advantage of higher switching rates for organelle investigation [57] (see also Section 4). Life imaging with STORM uses different strategies based on organic dyes, e.g. clathrin-coated pits were labeled indirectly with Alexa647-transferrin conjugates and composite images were obtained at 0.5 s acquisition time and 25 nm lateral resolution [45]. Compared to video rate STED, this corresponds to ~10-times slower acquisition rates. Notably, STORM in live cells was extended to dual-color labeling with transferrin-conjugates and SNAP-tag labeling of clathrin by electroporation [45]. Alternatively, a growing number of photo-switchable and inactivatable FPs may facilitate live cell labeling for stochastic readout. Live cell imaging with PALM achieved acquisition times of 25 s at 60 nm resolution for adhesion molecules using photon-resistant secondary cell lines [43], and clustering of a viral membrane protein was assessed with 40 nm resolution [81]. Furthermore, dual-color superresolution imaging of FPs was initially shown in fixed samples for adhesion complexes at 20–30 nm resolution using acquisition times of 5–30 min [82].

## 7. STED imaging of remodeled T-tubule membrane structures

We have recently demonstrated STED microscopy for intact T-tubule (TT) membrane structures, which included hollow sections of membrane structures deep inside living cardiac myocytes [4], clearly beyond the reach of conventional imaging techniques. Previous studies have extended the analysis of TTs to different levels including network analysis in 3D [70,71] or 2D [63,68], and to average TT parameters like diameters [83]. Intuitively, the most reliable quantitative assessment of complex membrane structures can be expected when the physiological cell conditions are well preserved during imaging. For this, live staining with membrane localized dyes has universal appeal and offers clear advantages for structure localization and dye access [57,63,67,69–71]. Considering ultrastructural EM analysis of cardiac couplons, thin cryosections are a necessary prerequisite [61,62]. Notably, EM studies reported somewhat variable TT cross-section sizes of 150–200 nm in cat heart which depend on fixation methods, which are clearly below the resolution limit of conventional light microscopy (Fig. 1A) [83]. Accordingly, confocal studies of small structural TT changes in heart disease were likely limited by the resolution barrier. On the other hand, microscale spatial network reorganization has been identified as a potential excitation–contraction uncoupling mechanism in heart disease [68]. Subsequently, indirect analysis of cell-wide TT striation patterns [63,68] has become a common and reliable strategy to characterize disease changes. A pioneering study based on two-photon excitation even visualized the 3D morphology of the TT network and analyzed TT sizes based on volume labeling and mathematical processing of diffraction-limited data [71].

Applying STED superresolution microscopy to living cardiomyocytes, we identified previously not recognized architectural details using quantitative analysis strategies each for individual TT elements and the cell-wide membrane network (Fig. 3), and identified differential changes early post-MI [4]. Cardiac myocytes from post-MI mouse hearts were stained with the membrane probe di-8-ANEPPS and imaged up to 8 μm deep intracellular from the surface (Fig. 2A *center*). Using STED, sharper TT membrane images with a significantly smaller cross-section area (~40% reduced) were obtained when directly compared to confocal images (Fig. 2A *center left*). Apparently, only STED resolved hollow membrane rings (cross section) and tubes (long section) depending on the orientation of the optical plane relative to individual TT elements (Fig. 3). Furthermore, analysis of individual TT cross-sections identified proliferative changes (Fig. 2A *center*), which at the level of the TT network increased the total length and the branching complexity early during the development of heart failure [4]. STED detected frequent, abnormally shaped TT components with grossly enlarged morphologies at network intersections post-MI (Fig. 2A *center left*), further suggesting proliferative membrane remodeling as the cause of increased network complexity early during HF development. Notably, the post-MI grossly enlarged TT membrane structures were not resolved by confocal imaging. Furthermore, confocal line scan imaging for combined $Ca^{2+}$ and TT structure–function analysis showed that the spatial TT changes have important functional consequences as evidenced by dyssynchronous $Ca^{2+}$ release [4]. In summary, the observed membrane staining and brightness of di-8-ANEPPS proved to be compatible with deep intracellular STED imaging in cardiomyocytes. This strategy using a directly intercalated membrane dye for STED superresolution microscopy can be readily extended to other live organotypic cells or further questions about intact membranes.

## 8. Single-molecule imaging of the RyR2 super-complex in fixed cardiomyocytes

Superresolution microscopy has significantly contributed to our understanding of the organization of cardiac ryanodine receptors (RyR2s) and associated proteins [6]. RyR2 functions as the main intracellular $Ca^{2+}$ release channel, occurring in clusters located at the

CRUs. While the exact nature of RyR2 channel organization inside clusters remains unclear, highly ordered cluster architectures were previously suggested based on in vitro EM studies showing lattice formations, consistent with EM model extrapolations from cryosection data of cardiomyocytes [61,84]. Notably, coupled gating of small numbers of RyR2 channels was identified by lipid bilayer recording, suggesting an important control mechanism of channel clustering for $Ca^{2+}$ release [85]. Analysis of thin EM cryosections from different species led to estimates of 90–270 RyR2s per cluster assuming a model of orderly filled, symmetric cluster architectures [61]. Cluster estimates deduced from confocal images suggested typical sizes of ~100 RyR2 channels [86]. In contrast, 3D electron microscopy provided a different model where approximately two thirds of the dyadic subspace contained clusters with 15 or more RyR2 channels [62].

However, the prevailing model of relatively large and symmetric RyR2 super-clusters has been challenged recently by superresolution images based on stochastic readout. Baddeley et al. reported that RyR2 clusters show a near exponential size distribution with an average cluster size of ~14 channels [6]. These clusters resembled irregular, elongated or partly circular shapes (Fig. 2B *lower*) [6]. Baddeley et al. concluded that the observed cluster size distribution may reflect a stochastic assembly process which includes super-clusters. In this study single-molecule localization microscopy at ~30 nm lateral resolution was based on an approach the authors have termed reversible photobleaching (RPM), which is essentially the same as the method called GSDIM [13,14] or dSTORM [87,88]. Due to total internal reflection (TIRF) illumination, the imaging was limited to RyR2 proteins at the cell surface of fixed cardiomyocytes. Recently, this strategy was extended to dual-color imaging based on near-infrared Alexa-fluor dyes for reversible photochemical conversion using a reducing mounting medium [15]. While confocal studies have suggested physical interactions of RyR2 and junctophilin-2 (JPH2), the exact in situ distribution of the proteins was not known [89]. Superresolution analysis of RyR2 and JPH2 showed the relative distributions in the junctional space (Fig. 2B *lower right*) [5]. Importantly, decreased levels of the JPH2 protein have been shown to destabilize the dyadic CRU architecture and $Ca^{2+}$ release [90]. JPH2 is downregulated in heart failure, which we have recently confirmed in a myocardial infarct model [4]. In addition, only a small fraction (5%) of caveolin-3 was colocalized with RyR2 clusters in superresolution images, while confocal studies overestimated the degree of colocalization by ~6-fold due to optical blurring of these paralocalized proteins [15]. In summary, while IF studies of protein super-clusters and specialized subcellular structures will necessarily experience limitations (see also Section 2), these strategies will continue to contribute to superresolution insight.

## 9. Future cardiac superresolution questions

Our cardiac superresolution survey showed that intact cell membranes and protein clusters are important areas for superresolution imaging. This reflects genuine questions about cardiac cell biology, where distinct membrane nanodomains or compartments exist, and often at a high spatial density in a given cell. Superresolution microscopy has already led to a new interpretation of the organization of CRUs [5,6,15,44]. Yet, the precise molecular organization of RyR2 receptors within super-clusters containing a high density of channel proteins still has to be resolved. Furthermore, we consider functional correlations of $Ca^{2+}$ signals important to reach new insight about the physiological CRU architecture and changes in disease. Notably, instructive analytical examples about protein clusters exist outside the cardiac field including the organization of synaptotagmin and syntaxin-1 clusters [45,91,92], or the organization of membrane domains containing a high density of ion channels like nicotinic acetylcholine and AMPA receptors [93,94].

Furthermore, superresolution microscopy is ideally positioned to resolve local membrane structures and their relation with organelles, e.g. parts of the SR/ER membranes in close proximity with mitochondria in cardiomyocytes and potential reciprocal signaling mechanisms [95,96]. Accordingly, established superresolution strategies for mitochondria and lipid nanodomains are of relevance [29,32,39,46,83,97,98]. Recent developments further support 3D superresolution insight which can be applied to study complex architectures of surface structures like T-tubule orifices or the nanodomain organization of the SR/ER membrane network and organelles [4,57]. In addition, the intercalated disc is an important structure harboring a dense molecular organization of intercellular contact zones. Accordingly, superresolution studies of adhesion complexes in fixed and living cells [39,43,46,82] have clearly outlined the potential for analogous approaches to study cardiac intercalated disc complexes. Furthermore, cytoskeletal filament structures have been successfully imaged by superresolution [19,35,44,82], which can be extended to the organization of cellular nanodomains and their dynamic control during cell stretch.

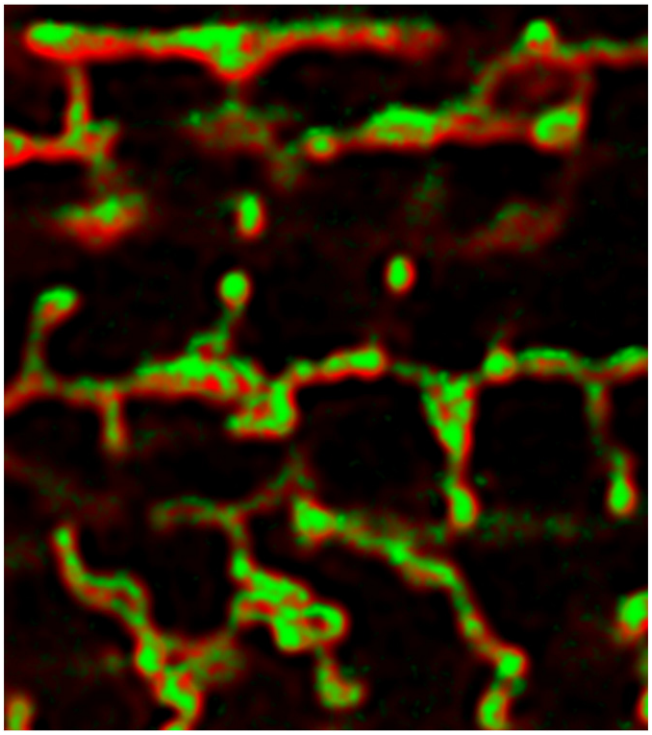

**Fig. 3.** Live cell T-tubule membrane structures after myocardial infaction. Combined image presention by overlaying STED and confocal imaging data of the same sample showing the membrane network of T-tubule structures and its changes 8 weeks after myocardial infarction. The conventional, diffraction limited confocal fluorescence image information (red) shows the effect of blurring of the membrane signal by light diffraction. In contrast, the overlaid superresolution signal (green) captured by Stimulated Emission Depletion (STED) microscopy reveals sharper membrane structures and many additional details. Here, the difference between the red and green fluorescent signals highlights the improved contrast and resolution achieved for a complex imaging object, the excitable membrane structures of living cardiac myocytes. This represents the first visualization of diseased membranes in cardiac cells by a targeted readout for superresolution imaging, identifying differential local mechanisms of post-MI membrane reorganization. The width of the image corresponds to 3 sarcomere units (~6 μm) and the horizontal orientation corresponds to the longitudinal cell axis.

## 10. Summary and outlook

Studying intricate physiological architectures and pathological changes of membrane nanodomains is an important and intrinsically motivated topic of research. Clearly, fluorescence superresolution microscopy or nanoscopy has already started to transform cardiac research. Limitations from confocal blurring can be avoided, and superresolution strategies improve the imaging of detailed and heterogeneous molecular signal patterns by several-fold increased resolution in cells. Apart from the apparent qualitative improvement

provided by superresolution imaging, it appears timely to reassess previous diffraction limited results by existing state-of-the-art superresolution approaches including advantageous new labeling techniques. Physiologically relevant, complex membrane structures like T-tubules with functionally important substructures motivate important questions, which include the vast area of membrane associated proteins, the organization of super-complexes and organelles. Additional improvements in FPs hold great promise for further advances in superresolution imaging, both through targeted and stochastic readouts in living cells. Furthermore, previously unattainable superresolution information and mathematical modeling of local subcellular structure–function relations are just starting to complement and invigorate entirely new approaches in cardiac cell biology.

## Non-standard abbreviations and acronyms

| | |
|---|---|
| BALM | bleaching/blinking assisted localization microscopy |
| CRU | Calcium Release Unit |
| FPALM | fluorescence photoactivation localization microscopy |
| GSDIM | ground-state-depletion with individual molecule return microscopy |
| PALM | photo-activation localization microscopy |
| PALMIRA | PALM with independently running acquisition |
| RESOLFT | reversible optically-linear fluorescence transitions microscopy |
| RyR1 | ryanodine receptor isoform 1, skeletal muscle type |
| RyR2 | ryanodine receptor isoform 2, cardiac muscle type |
| SIM | structured illumination microscopy |
| SSIM | saturated structured illumination microscopy |
| STED | stimulated emission depletion microscopy |
| (d) STORM | (direct) stochastic optical reconstruction microscopy |
| TT | transverse tubule or T-tubule |
| FP | fluorescent protein |
| IF | immunofluorescence |

## Disclosure statement

The authors declare that no conflict of interest exists.

## Acknowledgments

Sources of funding: This work received support through Deutsche Forschungsgemeinschaft (KFO 155 LE 1313/2 to SEL; SFB 1002 to SWH and SEL); a Halbach Foundation award to SEL; and a DAAD exchange program supporting TK at the University of Maryland. The research leading to these results has received funding from the European Community's Seventh Framework Program FP7/2007-2013 under grant agreement no. HEALTH-F2-2009-241526, EUTrigTreat (to SEL).

## References

[1] Huang B, Bates M, Zhuang X. Super-resolution fluorescence microscopy. Annu Rev Biochem 2009;78:993–1016.
[2] Schermelleh L, Heintzmann R, Leonhardt H. A guide to super-resolution fluorescence microscopy. J Cell Biol Jul 26 2010;190(2):165–75.
[3] Hell SW. Far-field optical nanoscopy. Science May 25 2007;316(5828):1153–8.
[4] Wagner E, Lauterbach M, Kohl T, Westphal V, Williams GS, Steinbrecher JH, et al. STED live cell super-resolution imaging shows proliferative remodeling of T-tubule membrane structures after myocardial infarction. Circ Res Aug 3 2012;111(4):402–14.
[5] Jayasinghe ID, Baddeley D, Kong CH, Wehrens XH, Cannell MB, Soeller C. Nanoscale organization of junctophilin-2 and ryanodine receptors within peripheral couplings of rat ventricular cardiomyocytes. Biophys J Mar 7 2012;102(5):L19–21.
[6] Baddeley D, Jayasinghe ID, Lam L, Rossberger S, Cannell MB, Soeller C. Optical single-channel resolution imaging of the ryanodine receptor distribution in rat cardiac myocytes. Proc Natl Acad Sci U S A Dec 29 2009;106(52):22275–80.
[7] Hell SW, Wichmann J. Breaking the diffraction resolution limit by stimulated emission: stimulated-emission-depletion fluorescence microscopy. Opt Lett Jun 1 1994;19(11):780–2.
[8] Klar TA, Hell SW. Subdiffraction resolution in far-field fluorescence microscopy. Opt Lett Jul 15 1999;24(14):954–6.
[9] Hofmann M, Eggeling C, Jakobs S, Hell SW. Breaking the diffraction barrier in fluorescence microscopy at low light intensities by using reversibly photoswitchable proteins. Proc Natl Acad Sci U S A Dec 6 2005;102(49):17565–9.
[10] Gustafsson MG. Surpassing the lateral resolution limit by a factor of two using structured illumination microscopy. J Microsc May 2000;198(Pt. 2):82–7.
[11] Heintzmann R, Jovin TM, Cremer C. Saturated patterned excitation microscopy—a concept for optical resolution improvement. J Opt Soc Am A Opt Image Sci Vis Aug 2002;19(8):1599–609.
[12] Gustafsson MG. Nonlinear structured-illumination microscopy: wide-field fluorescence imaging with theoretically unlimited resolution. Proc Natl Acad Sci U S A Sep 13 2005;102(37):13081–6.
[13] Bock H, Geisler C, Wurm C, Jakobs S, Schonle A, Egner A, et al. Two-color far-field fluorescence nanoscopy based on photoswitching emitters. Appl Phys B 2007;88:161–5.
[14] Folling J, Bossi M, Bock H, Medda R, Wurm CA, Hein B, et al. Fluorescence nanoscopy by ground-state depletion and single-molecule return. Nat Methods Nov 2008;5(11):943–5.
[15] Baddeley D, Crossman D, Rossberger S, Cheyne JE, Montgomery JM, Jayasinghe ID, et al. 4D super-resolution microscopy with conventional fluorophores and single wavelength excitation in optically thick cells and tissues. PLoS One 2011;6(5):e20645.
[16] Bretschneider S, Eggeling C, Hell SW. Breaking the diffraction barrier in fluorescence microscopy by optical shelving. Phys Rev Lett May 25 2007;98(21):218103.
[17] Bingen P, Reuss M, Engelhardt J, Hell SW. Parallelized STED fluorescence nanoscopy. Opt Express Nov 21 2011;19(24):23716–26.
[18] Schwentker MA, Bock H, Hofmann M, Jakobs S, Bewersdorf J, Eggeling C, et al. Wide-field subdiffraction RESOLFT microscopy using fluorescent protein photoswitching. Microsc Res Tech Mar 2007;70(3):269–80.
[19] Donnert G, Keller J, Medda R, Andrei MA, Rizzoli SO, Luhrmann R, et al. Macromolecular-scale resolution in biological fluorescence microscopy. Proc Natl Acad Sci U S A Aug 1 2006;103(31):11440–5.
[20] Willig KI, Nagerl UV. Stimulated emission depletion (STED) imaging of dendritic spines in living hippocampal slices. Cold Spring Harb Protoc May 2012;2012(5).
[21] Vicidomini G, Moneron G, Han KY, Westphal V, Ta H, Reuss M, et al. Sharper low-power STED nanoscopy by time gating. Nat Methods Jul 2011;8(7):571–3.
[22] Willig KI, Kellner RR, Medda R, Hein B, Jakobs S, Hell SW. Nanoscale resolution in GFP-based microscopy. Nat Methods Sep 2006;3(9):721–3.
[23] Nagerl UV, Willig KI, Hein B, Hell SW, Bonhoeffer T. Live-cell imaging of dendritic spines by STED microscopy. Proc Natl Acad Sci U S A Dec 2 2008;105(48):18982–7.
[24] Moneron G, Medda R, Hein B, Giske A, Westphal V, Hell SW. Fast STED microscopy with continuous wave fiber lasers. Opt Express Jan 18 2010;18(2):1302–9.
[25] Meyer L, Wildanger D, Medda R, Punge A, Rizzoli SO, Donnert G, et al. Dual-color STED microscopy at 30-nm focal-plane resolution. Small Aug 2008;4(8):1095–100.
[26] Rankin BR, Kellner RR, Hell SW. Stimulated-emission-depletion microscopy with a multicolor stimulated-Raman-scattering light source. Opt Lett Nov 1 2008;33(21):2491–3.
[27] Wildanger D, Medda R, Kastrup L, Hell SW. A compact STED microscope providing 3D nanoscale resolution. J Microsc Oct 2009;236(1):35–43.
[28] Hein B, Willig KI, Hell SW. Stimulated emission depletion (STED) nanoscopy of a fluorescent protein-labeled organelle inside a living cell. Proc Natl Acad Sci September 23 2008;105(38):14271–6.
[29] Donnert G, Keller J, Wurm CA, Rizzoli SO, Westphal V, Schonle A, et al. Two-color far-field fluorescence nanoscopy. Biophys J Apr 15 2007;92(8):L67–9.
[30] Schmidt R, Wurm CA, Jakobs S, Engelhardt J, Egner A, Hell SW. Spherical nanosized focal spot unravels the interior of cells. Nat Methods Jun 2008;5(6):539–44.
[31] Buckers J, Wildanger D, Vicidomini G, Kastrup L, Hell SW. Simultaneous multi-lifetime multi-color STED imaging for colocalization analyses. Opt Express Feb 14 2011;19(4):3130–43.
[32] Neumann D, Buckers J, Kastrup L, Hell SW, Jakobs S. Two-color STED microscopy reveals different degrees of colocalization between hexokinase-I and the three human VDAC isoforms. PMC Biophys 2010;3(1):4.
[33] Arlt J, Padgett MJ. Generation of a beam with a dark focus surrounded by regions of higher intensity: the optical bottle beam. Opt Lett Feb 15 2000;25(4):191–3.
[34] Klar TA, Jakobs S, Dyba M, Egner A, Hell SW. Fluorescence microscopy with diffraction resolution barrier broken by stimulated emission. Proc Natl Acad Sci U S A Jul 18 2000;97(15):8206–10.
[35] Willig KI, Harke B, Medda R, Hell SW. STED microscopy with continuous wave beams. Nat Methods Nov 2007;4(11):915–8.
[36] Harke B, Ullal CK, Keller J, Hell SW. Three-dimensional nanoscopy of colloidal crystals. Nano Lett May 2008;8(5):1309–13.
[37] Schermelleh L, Carlton PM, Haase S, Shao L, Winoto L, Kner P, et al. Subdiffraction multicolor imaging of the nuclear periphery with 3D structured illumination microscopy. Science Jun 6 2008;320(5881):1332–6.
[38] Rust MJ, Bates M, Zhuang X. Sub-diffraction-limit imaging by stochastic optical reconstruction microscopy (STORM). Nat Methods Oct 2006;3(10):793–5.
[39] Betzig E, Patterson GH, Sougrat R, Lindwasser OW, Olenych S, Bonifacino JS, et al. Imaging intracellular fluorescent proteins at nanometer resolution. Science Sep 15 2006;313(5793):1642–5.
[40] Hess ST, Girirajan TP, Mason MD. Ultra-high resolution imaging by fluorescence photoactivation localization microscopy. Biophys J Dec 1 2006;91(11):4258–72.
[41] Egner A, Geisler C, von Middendorff C, Bock H, Wenzel D, Medda R, et al. Fluorescence nanoscopy in whole cells by asynchronous localization of photoswitching emitters. Biophys J Nov 1 2007;93(9):3285–90.

[42] Burnette DT, Sengupta P, Dai Y, Lippincott-Schwartz J, Kachar B. Bleaching/blinking assisted localization microscopy for superresolution imaging using standard fluorescent molecules. Proc Natl Acad Sci U S A Dec 27 2011;108(52):21081–6.
[43] Shroff H, Galbraith CG, Galbraith JA, Betzig E. Live-cell photoactivated localization microscopy of nanoscale adhesion dynamics. Nat Methods May 2008;5(5):417–23.
[44] Baddeley D, Cannell M, Soeller C. Three-dimensional sub-100 nm super-resolution imaging of biological samples using a phase ramp in the objective pupil. Nano Res 2011;4(6):589–98.
[45] Jones SA, Shim SH, He J, Zhuang X. Fast, three-dimensional super-resolution imaging of live cells. Nat Methods Jun 2011;8(6):499–508.
[46] Kanchanawong P, Shtengel G, Pasapera AM, Ramko EB, Davidson MW, Hess HF, et al. Nanoscale architecture of integrin-based cell adhesions. Nature Nov 25 2010;468(7323):580–4.
[47] Churchman LS, Okten Z, Rock RS, Dawson JF, Spudich JA. Single molecule high-resolution colocalization of Cy3 and Cy5 attached to macromolecules measures intramolecular distances through time. Proc Natl Acad Sci U S A Feb 1 2005;102(5):1419–23.
[48] Lacoste TD, Michalet X, Pinaud F, Chemla DS, Alivisatos AP, Weiss S. Ultrahigh-resolution multicolor colocalization of single fluorescent probes. Proc Natl Acad Sci U S A Aug 15 2000;97(17):9461–6.
[49] Gordon MP, Ha T, Selvin PR. Single-molecule high-resolution imaging with photobleaching. Proc Natl Acad Sci U S A Apr 27 2004;101(17):6462–5.
[50] Qu X, Wu D, Mets L, Scherer NF. Nanometer-localized multiple single-molecule fluorescence microscopy. Proc Natl Acad Sci U S A Aug 3 2004;101(31):11298–303.
[51] Bates M, Huang B, Dempsey GT, Zhuang X. Multicolor super-resolution imaging with photo-switchable fluorescent probes. Science Sep 21 2007;317(5845):1749–53.
[52] Bates M, Dempsey GT, Chen KH, Zhuang X. Multicolor super-resolution fluorescence imaging via multi-parameter fluorophore detection. Chemphyschem Jan 16 2012;13(1):99–107.
[53] Tynan CJ, Clarke DT, Coles BC, Rolfe DJ, Martin-Fernandez ML, Webb SE. Multicolour single molecule imaging in cells with near infra-red dyes. PLoS One 2012;7(4):e36265.
[54] Fernandez-Suarez M, Ting AY. Fluorescent probes for super-resolution imaging in living cells. Nat Rev Mol Cell Biol Dec 2008;9(12):929–43.
[55] Ries J, Kaplan C, Platonova E, Eghlidi H, Ewers H. A simple, versatile method for GFP-based super-resolution microscopy via nanobodies. Nat Methods Jun 2012;9(6):582–4.
[56] Guo T, Cornea RL, Huke S, Camors E, Yang Y, Picht E, et al. Kinetics of FKBP12.6 binding to ryanodine receptors in permeabilized cardiac myocytes and effects on Ca sparks. Circ Res Jun 11 2010;106(11):1743–52.
[57] Shim SH, Xia C, Zhong G, Babcock HP, Vaughan JC, Huang B, et al. Super-resolution fluorescence imaging of organelles in live cells with photoswitchable membrane probes. Proc Natl Acad Sci U S A Aug 28 2012;109(35):13978–83.
[58] Lau L, Lee YL, Sahl SJ, Stearns T, Moerner WE. STED microscopy with optimized labeling density reveals 9-fold arrangement of a centriole protein. Biophys J Jun 20 2012;102(12):2926–35.
[59] Parfenov AS, Salnikov V, Lederer WJ, Lukyanenko V. Aqueous diffusion pathways as a part of the ventricular cell ultrastructure. Biophys J Feb 1 2006;90(3):1107–19.
[60] Protasi F, Franzini-Armstrong C, Flucher BE. Coordinated incorporation of skeletal muscle dihydropyridine receptors and ryanodine receptors in peripheral couplings of BC3H1 cells. J Cell Biol May 19 1997;137(4):859–70.
[61] Franzini-Armstrong C, Protasi F, Ramesh V. Shape, size, and distribution of $Ca^{2+}$ release units and couplons in skeletal and cardiac muscles. Biophys J 1999;77(3):1528–39.
[62] Hayashi T, Martone ME, Yu Z, Thor A, Doi M, Holst MJ, et al. Three-dimensional electron microscopy reveals new details of membrane systems for $Ca^{2+}$ signaling in the heart. J Cell Sci April 1 2009;122(7):1005–13.
[63] Crossman DJ, Ruygrok PN, Soeller C, Cannell MB. Changes in the organization of excitation–contraction coupling structures in failing human heart. PLoS One 2011;6(3):e17901.
[64] Scriven DR, Asghari P, Schulson MN, Moore ED. Analysis of Cav1.2 and ryanodine receptor clusters in rat ventricular myocytes. Biophys J Dec 15 2010;99(12):3923–9.
[65] Schulson MN, Scriven DR, Fletcher P, Moore ED. Couplons in rat atria form distinct subgroups defined by their molecular partners. J Cell Sci Apr 1 2011;124(Pt. 7):1167–74.
[66] Scriven DR, Dan P, Moore ED. Distribution of proteins implicated in excitation–contraction coupling in rat ventricular myocytes. Biophys J Nov 2000;79(5):2682–91.
[67] Jayasinghe ID, Cannell MB, Soeller C. Organization of ryanodine receptors, transverse tubules, and sodium–calcium exchanger in rat myocytes. Biophys J Nov 18 2009;97(10):2664–73.
[68] Song LS, Sobie EA, McCulle S, Lederer WJ, Balke CW, Cheng H. Orphaned ryanodine receptors in the failing heart. Proc Natl Acad Sci U S A Mar 14 2006;103(11):4305–10.
[69] Edwards JN, Cully TR, Shannon TR, Stephenson DG, Launikonis BS. Longitudinal and transversal propagation of excitation along the tubular system of rat fast-twitch muscle fibres studied by high speed confocal microscopy. J Physiol Feb 1 2012;590(Pt. 3):475–92.
[70] Savio-Galimberti E, Frank J, Inoue M, Goldhaber JI, Cannell MB, Bridge JH, et al. Novel features of the rabbit transverse tubular system revealed by quantitative analysis of three-dimensional reconstructions from confocal images. Biophys J Aug 2008;95(4):2053–62.
[71] Soeller C, Cannell MB. Examination of the transverse tubular system in living cardiac rat myocytes by 2-photon microscopy and digital image-processing techniques. Circ Res Feb 19 1999;84(3):266–75.
[72] Cheng H, Lederer WJ, Cannell MB. Calcium sparks: elementary events underlying excitation–contraction coupling in heart muscle. Science Oct 29 1993;262(5134):740–4.
[73] Gomez AM, Valdivia HH, Cheng H, Lederer MR, Santana LF, Cannell MB, et al. Defective excitation–contraction coupling in experimental cardiac hypertrophy and heart failure. Science May 2 1997;276(5313):800–6.
[74] Cheng H, Lederer WJ. Calcium sparks. Physiol Rev October 1 2008;88(4):1491–545.
[75] Sacconi L, Ferrantini C, Lotti J, Coppini R, Yan P, Loew LM, et al. Action potential propagation in transverse-axial tubular system is impaired in heart failure. Proc Natl Acad Sci U S A Apr 10 2012;109(15):5815–9.
[76] Westphal V, Rizzoli SO, Lauterbach MA, Kamin D, Jahn R, Hell SW. Video-rate far-field optical nanoscopy dissects synaptic vesicle movement. Science Apr 11 2008;320(5873):246–9.
[77] Berning S, Willig KI, Steffens H, Dibaj P, Hell SW. Nanoscopy in a living mouse brain. Science Feb 3 2012;335(6068):551.
[78] Grotjohann T, Testa I, Leutenegger M, Bock H, Urban NT, Lavoie-Cardinal F, et al. Diffraction-unlimited all-optical imaging and writing with a photochromic GFP. Nature 2011;478(7368):204–8.
[79] Willig KI, Stiel AC, Brakemann T, Jakobs S, Hell SW. Dual-label STED nanoscopy of living cells using photochromism. Nano Lett Sep 14 2011;11(9):3970–3.
[80] Pellett PA, Sun X, Gould TJ, Rothman JE, Xu MQ, Correa Jr IR, et al. Two-color STED microscopy in living cells. Biomed Opt Express Aug 1 2011;2(8):2364–71.
[81] Hess ST, Gould TJ, Gudheti MV, Maas SA, Mills KD, Zimmerberg J. Dynamic clustered distribution of hemagglutinin resolved at 40 nm in living cell membranes discriminates between raft theories. Proc Natl Acad Sci U S A Oct 30 2007;104(44):17370–5.
[82] Shroff H, Galbraith CG, Galbraith JA, White H, Gillette J, Olenych S, et al. Dual-color superresolution imaging of genetically expressed probes within individual adhesion complexes. Proc Natl Acad Sci U S A Dec 18 2007;104(51):20308–13.
[83] Fawcett DW, McNutt NS. The ultrastructure of the cat myocardium. I. Ventricular papillary muscle. J Cell Biol Jul 1969;42(1):1–45.
[84] Yin CC, Lai FA. Intrinsic lattice formation by the ryanodine receptor calcium-release channel. Nat Cell Biol Sep 2000;2(9):669–71.
[85] Marx SO, Gaburjakova J, Gaburjakova M, Henrikson C, Ondrias K, Marks AR. Coupled gating between cardiac calcium release channels (ryanodine receptors). Circ Res June 8 2001;88(11):1151–8.
[86] Chen-Izu Y, McCulle SL, Ward CW, Soeller C, Allen BM, Rabang C, et al. Three-dimensional distribution of ryanodine receptor clusters in cardiac myocytes. Biophys J Jul 1 2006;91(1):1–13.
[87] Heilemann M, van de Linde S, Schuttpelz M, Kasper R, Seefeldt B, Mukherjee A, et al. Subdiffraction-resolution fluorescence imaging with conventional fluorescent probes. Angew Chem Int Ed Engl 2008;47(33):6172–6.
[88] van de Linde S, Sauer M, Heilemann M. Subdiffraction-resolution fluorescence imaging of proteins in the mitochondrial inner membrane with photoswitchable fluorophores. J Struct Biol Dec 2008;164(3):250–4.
[89] Ziman AP, Gomez-Viquez NL, Bloch RJ, Lederer WJ. Excitation–contraction coupling changes during postnatal cardiac development. J Mol Cell Cardiol Feb 2010;48(2):379–86.
[90] van Oort RJ, Garbino A, Wang W, Dixit SS, Landstrom AP, Gaur N, et al. Disrupted junctional membrane complexes and hyperactive ryanodine receptors after acute junctophilin knockdown in mice. Circulation Mar 8 2011;123(9):979–88.
[91] Willig KI, Rizzoli SO, Westphal V, Jahn R, Hell SW. STED microscopy reveals that synaptotagmin remains clustered after synaptic vesicle exocytosis. Nature Apr 13 2006;440(7086):935–9.
[92] Sieber JJ, Willig KI, Kutzner C, Gerding-Reimers C, Harke B, Donnert G, et al. Anatomy and dynamics of a supramolecular membrane protein cluster. Science Aug 24 2007;317(5841):1072–6.
[93] Kellner RR, Baier CJ, Willig KI, Hell SW, Barrantes FJ. Nanoscale organization of nicotinic acetylcholine receptors revealed by stimulated emission depletion microscopy. Neuroscience Jan 5 2007;144(1):135–43.
[94] Meyer AC, Frank T, Khimich D, Hoch G, Riedel D, Chapochnikov NM, et al. Tuning of synapse number, structure and function in the cochlea. Nat Neurosci Apr 2009;12(4):444–53.
[95] Franzini-Armstrong C. ER-mitochondria communication. How privileged? Physiology (Bethesda) Aug 2007;22:261–8.
[96] Chikando AC, Kettlewell S, Williams GS, Smith G, Lederer WJ. $Ca^{2+}$ dynamics in the mitochondria—state of the art. J Mol Cell Cardiol Nov 2011;51(5):627–31.
[97] Wurm CA, Neumann D, Lauterbach MA, Harke B, Egner A, Hell SW, et al. Nanoscale distribution of mitochondrial import receptor Tom20 is adjusted to cellular conditions and exhibits an inner-cellular gradient. Proc Natl Acad Sci U S A Aug 16 2011;108(33):13546–51.
[98] Eggeling C, Ringemann C, Medda R, Schwarzmann G, Sandhoff K, Polyakova S, et al. Direct observation of the nanoscale dynamics of membrane lipids in a living cell. Nature Feb 26 2009;457(7233):1159–62.
[99] Schmidt R, Wurm CA, Punge A, Egner A, Jakobs S, Hell SW. Mitochondrial cristae revealed with focused light. Nano Lett Jun 2009;9(6):2508–10.
[100] Serysheva II, Ludtke SJ, Baker ML, Cong Y, Topf M, Eramian D, et al. Subnanometer-resolution electron cryomicroscopy-based domain models for the cytoplasmic region of skeletal muscle RyR channel. Proc Natl Acad Sci U S A Jul 15 2008;105(28):9610–5.
[101] Yang F, Moss LG, Phillips GN. The molecular structure of green fluorescent protein. Nat Biotechnol 1996;14(10):1246–51.